Supporting Information

Regulating Coordination Environment of Co single-atom through Ni/Co Sulphides synergistic Heterointerfaces towards Efficient Bifunctional Oxygen Electrocatalysts

Zhi-da Wang,[a] Pei-tao Liu,[a] Chong-yang Yang,[a] Zi-han Zhan,[a] Yu Qian,[a] Yan-qing Zu,[a] Xiao-dong Li[a] and Ai-ling Feng*[a]*

[a] Institute of Physics and Optoelectronics Technology, Baoji University of Arts and Sciences, Baoji 721016, PR China

* E-mail: liupt@bjwlxy.edu.cn (PTL); ailingfeng@bjwlxy.edu.cn (ALF).

Section 1. Experimental details.

Chemicals: Cobalt (II) nitrate hexahydrate [$Co(NO_3)_2 \cdot 6H_2O$, 99 %] (AR, Aladdin Reagent Co., Ltd.), Nickel (II) nitrate hexahydrate [$Ni(NO_3)_2 \cdot 6H_2O$,99 %] (AR, Aladdin Reagent Co., Ltd.), methanol [C_2H_6O, 99 %] (AR, Macklin Reagent Co., Ltd.), ethanol [C_2H_5OH, 99 %] (AR, Macklin Reagent Co., Ltd.), 2-methylimidazole [$C_4H_6N_2$, 99 %] (AR, Aladdin Reagent Co., Ltd.), thiourea [CH_4N_2S, 98 %] (AR, Aladdin Reagent Co., Ltd.), Tetraethyl orthosilicate [$C_8H_{20}O_4Si$, 99 %] (AR, Aladdin Reagent Co., Ltd.), ammonia solution [NH_4OH, 30 %] (AR, Aladdin Reagent Co., Ltd.), potassium hydroxide [KOH, 99 %] (AR, Aladdin Reagent Co., Ltd.), hydrochloric Acid [HCl, 37 %] (AR, Aladdin Reagent Co., Ltd.), zinc acetate [$C_4H_6O_4Zn \cdot 2H_2O$, 99 %] (AR, Aladdin Reagent Co., Ltd.), Nafion-117 [$C_7HF_{13}O_5S$, 5 wt.%] (AR, Dupont USA Co.), N,N-Dimethylformamide [C_3H_7NO, 99 %] (AR, Aladdin Reagent Co., Ltd.), petroleum ether[C_3H_7NO, 99 %] (AR, Aladdin Reagent Co., Ltd.), Pt/C [20 %] (AR, Premetek Co.), Ir/C [20 %] (AR, Premetek Co.). All reagents were directly served as obtained without further depuration.

Synthesis of SiO_2: 8 mL of an ammonia solution was added to a mixture containing 40 mL of water with 400 mL of ethanol and stirred at 1000 rpm. Next, 15 mL of TEOS was dropwise added in the mixture, then left for 3 hours. The obtained solution was subsequently centrifuged and washed with DI water and ethanol several times. The yielded SiO_2 was dried in the oven at 60 °C over the night.

Synthesis of ZIF-67@SiO_2: Silica nanospheres (1g) was added in a solution of $Co(NO_3)_2 \cdot 6H_2O$ (6.552 g) dissolved in 80 mL of methanol and stirred for 20 min. In another beaker, 2-methylimidazole(7.938 g) was dissolved in 80 ml of methanol and stirred for 20 min. The above solutions were then mixed under vigorous stirring to form the dark purple liquid. Following a period of standing, a purple precipitate was obtained. The purple precipitate were repeatedly rinsed with de-ionized (DI) water and ethanol, followed by thorough drying in a drying oven. The resultant purple products was labeled as ZIF67@SiO_2. For comparison, ZIF-67 without the SiO_2 were prepared, following the same process.

Synthesis of Co_1/Ni_1-S: $Co(NO_3)_2 \cdot 6H_2O$ (6.75 g), $Ni(NO_3)_2 \cdot 6H_2O$ (6.75 g), and CH_4N_2S (13.5 g) were dissolved into 60 mL of DI water and stirred at 1500 rpm for 12 h , the dispersion transferred into a Teflon-lined stainless autoclave (volume of 100 mL), and heated at 220 ℃ for 24 h. Afterwards, the reaction system cooled down to 25 ℃. The black precipitate were repeatedly rinsed with DI water and ethanol, followed by thorough drying in a drying oven. The black products was denoted as Co_1/Ni_1-S. For comparison, the sample fabricated by using the same conditions with $Co(NO_3)_2 \cdot 6H_2O$ (6.75 g) and $Ni(NO_3)_2 \cdot 6H_2O$ (13.5 g) was named as Co_1/Ni_2-S, sample with $Co(NO_3)_2 \cdot 6H_2O$ (13.5 g) and $Ni(NO_3)_2 \cdot 6H_2O$ (6.75 g) was named as Co_2/Ni_1-S , sample without $Co(NO_3)_2 \cdot 6H_2O$ was named as Co_0/Ni_1-S and sample without $Ni(NO_3)_2 \cdot 6H_2O$ was named Co_1/Ni_0-S.

Synthesis of Ni_3S_2/Co_9S_8: Co_1/Ni_1-S (0.4g) were ground with mortar and pestle. To obtain the Ni_3S_2/Co_9S_8, the Co_1/Ni_1-S was pyrolyzed in N_2 atmosphere at 800 °C for 2 h with a ramping rate of 5 °C min^{-1} and cooled down to room temperature.

Synthesis of Co-NC: The ZIF-67 (1g) was pyrolyzed in N_2 atmosphere at 800 °C for 2 h with a ramping rate of 5 °C min^{-1}. After cooled down to room temperature, the obtained sample was denoted as Co-NC.

Synthesis of Ni_3S_2/Co_9S_8@Co-NC: The ZIF-67@SiO_2 (1g), Co_1/Ni_1-S (0.4g) were ground with mortar and pestle, affording the composite precursor ZIF-67@SiO_2@Co_1/Ni_1-S. To obtain the catalysts, the ZIF-

67@SiO_2@Co_1/Ni_1-S was pyrolyzed in N_2 atmosphere at 800 °C for 2 h with a ramping rate of 5 °C min^{-1}. After cooled down to room temperature, the obtained black solid products denoted as Co/Ni_3S_2/Co_9S_8/SiO_2@NC and etched with 4 M KOH solution for 24 h at room temperature. The black precipitate were repeatedly rinsed with DI water and 0.1 M HCl, followed by thorough drying in a drying oven. The resulting catalyst was denoted as Ni_3S_2/Co_9S_8@Co-NC. For comparison, the sample fabricated by using the same conditions with Co_2/Ni_1-S was named as Ni_3S_2/Co_9S_8@Co-NC-1, sample with Co_1/Ni_2-S was named as Ni_3S_2/Co_9S_8@Co-NC-2, sample with Co_1/Ni_0-S was named as Co_9S_8@Co-NC and sample with Co_0/Ni_1-S was named as Ni_3S_2@Co-NC.

Characterizations: The morphology of the samples were assessed using scanning electron microscopy (SEM; Hitachi Flex-2000, Japan). Transmission electron microscope and High-resolution TEM (TEM and HRTEM; JEOL JEM 2100F, Japan) were used to observe the morphology and structure of the products. And transmission electron microscope (TEM, thermoscientific spectra 300,USA) equipped with a high-angle annular dark field (HAADF) detector and a spherical aberration (Cs) probe corrector was employed to characterize the sample's morphology at the atomic level. Furthermore, we investigated the crystallographic and chemical states of the elements in the samples using powder X-ray diffraction measurement (XRD; Bruker D8, Karlsruhe, Germany) and X-ray photoelectron spectroscopy (XPS; Shimadzu Kratos AXIS Supratm, Japan). In-situ Raman (Horiba LabRAM HR Evolution, French) analysis is employed to examine the phase transition process of a given sample at varying potentials. The electron spin resonance (ESP/EPR; JEOL JES-FA300, Japan) method is utilized to identify and quantify the intermediates of the catalytic process of the samples, as well as to assess the extent of defects in the samples. The contact angle (KRUSS DSA25, Germany) is used to test the hydrophilic/hydrophobicity of the sample. Raman spectroscopy was conducted with a Renishaw in Via spectrometer at room temperature. The N_2 adsorption/desorption isotherms were collected at 80 °C by using a Micromeritics ASAP 2460.

Electrochemical measurement: The ORR and OER performances of the as-prepared catalysts on CHI 760E (Shanghai Chenhua Instrument Corporation, Shanghai, China) equipped with a three-electrode system in alkaline solutions. A platinum sheet was used as the counter electrode and Ag/AgCl as the reference electrode. The as-prepared samples mounted on a glassy carbon electrode (GC) or a rotating ring-disk electrode (RRDE) were used as the working electrode. All the measured potentials (vs Ag/AgCl) in this work were converted to a reversible hydrogen electrode (RHE) and iR corrected according to the Nernst equation ($E_{RHE} = E_{Ag/AgCl} + 0.197 + 0.059$ pH). To prepare the catalyst slurry, 3.0 mg of electrocatalyst was dispersed in 1460 μL N, N-dimethylformamide (DMF) and 40 μL Nafion solution (5.0 wt %; Sigma-Aldri**(c)** and ultrasonicated for 6 h. An aliquot of the catalytic ink (9 μL) was then dropped in a GC electrode (geometric area: 0.0706 cm^2) and dried at room temperature. For preparation of the ORR catalyst, the above catalytic ink was dropped in a rotating disk working electrode (RDE) with a loading amount of 0.2 mg/cm^2.

The number of electrons transferred (n) and H_2O_2 yield were calculated from the following equations:

$$n = \frac{4 \times I_d}{I_d + I_r/N} \quad (1)$$

$$H_2O_2\% = \frac{200 \times I_d}{I_r + I_d N} \quad (2)$$

where I_d is the disk current and I_r represents the ring current. N stands for the collection efficiency of the ring electrode (0.40).

Based on LSV curves with various rotating speeds, Koutecky-Levich (K-L) equation can be used to calculate the number of electrons transferred and the mass-transfer corrected kinetic current density J_K.

$$\frac{1}{J} = \frac{1}{J_K} + \frac{1}{J_L} = \frac{1}{J_K} + \frac{1}{B\omega^{1/2}} \quad (3)$$

$$B = 0.2nFC_0D_0^{2/3}\nu^{-1/6} \quad (4)$$

where J and J_L represent measured current density and diffusion-limiting current density, respectively. F is Faraday constant (F = 96485 C mol^{-1}). C_0 (1.2×10^{-6} mol cm^{-3}) and D_0 (1.9×10^{-5} cm^2 s^{-1}, 0.1 M KOH) represent the bulk concentration and diffusion coefficient of O_2, respectively. ν (0.01 cm^2 s^{-1}) is kinetic viscosity. 0.2 is constant when the unit of ω is revolutions per minute (r/min = rpm).

Turnover frequency (TOF) was calculated based on the following equation:

$$TOF = J \times S/(4 \times F \times n) \quad (5)$$

where J represent measured current density at η = 256 mV, S is surface area of sample electrode, the number 4 means 4 electrons mol^{-1} of O_2, F is Faraday constant (F = 96485 C mol^{-1}), and n is the moles of coated metal atom on the electrode calculated from m.

We used electrical double-layer capacitor(C_{dl}) to calculate electrochemical active surface area (ECSA). The ECSA is calculated as follows,

$$R_f = C_{dl}/C_s,\ ECSA = R_f/m \quad (6)$$

where C_S is the surface double layer capacitance of an ideal smooth oxide (60 μF cm^{-2})

Liquid Zn-air battery: The batteries tests were performed with homemade zinc-air battery using LAND CT3001A multi-channel battery testing system (WuHan LanDian Instruments). The air-electrode was made by drop-casting of the catalyst ink onto carbon cloth, then dried at room temperature, the catalyst loading was 2 mg cm^{-2}. A Zinc foil was used as an anode. The zinc-air battery was then assembled by filling the electrolyte (6 M KOH and 0.2 M Zn(A**(c)**$_2$) between the anode and the air-cathode, and was continuously pumped to the battery. For comparison, Pt/C and Ir/C were mixed at a mass ratio of 1:1 as air electrodes to fabricate zinc-air batteries.

Flexible all-solid-state Zn-air battery: Flexible ZABs were fabricated using polished zinc foil as the anode, the synthesized catalysts as the cathodes, and a gel polymer as solid electrolyte. The solid electrolyte was prepared as follow: polyvinyl alcohol (PVA) powder was added into 10 mL H_2O at 90 °C under an oil bath. Once the solution had slowly transformed into transparent gel, 1 mL of a high concentration alkali solution (18 M KOH with 0.02 M Zn(A**(c)**$_2$) was added to the gel. After 0.5 h of stirring, the mixture was poured onto a glass plate and placed in a freezer at -18 °C for 3 h.

The specific capacity for Zn-air battery was calculated by the equation below:

$$Specific\ capacity\ \left(mAh\ g^{-1}\right) = \frac{I_{dis} \times t}{m} \tag{7}$$

where I_{dis} represents the discharge current and t represents the service hours. m denotes the weight of Zn consumed.

Section 2. Supporting figures.

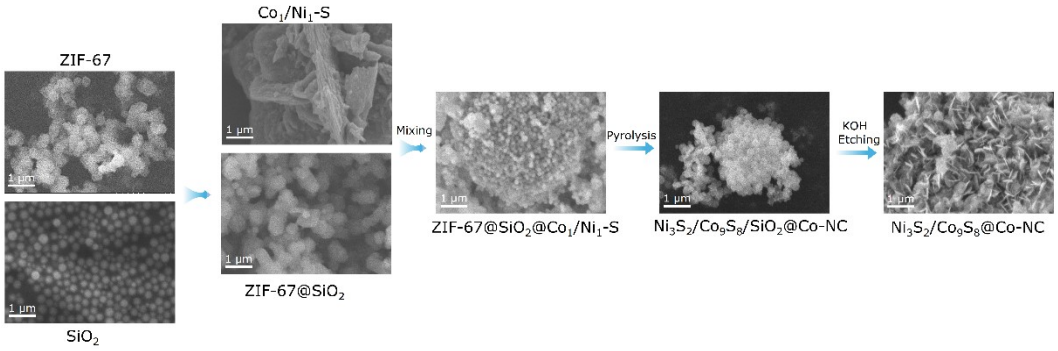

Fig. S1. SEM images of the products for each stage.

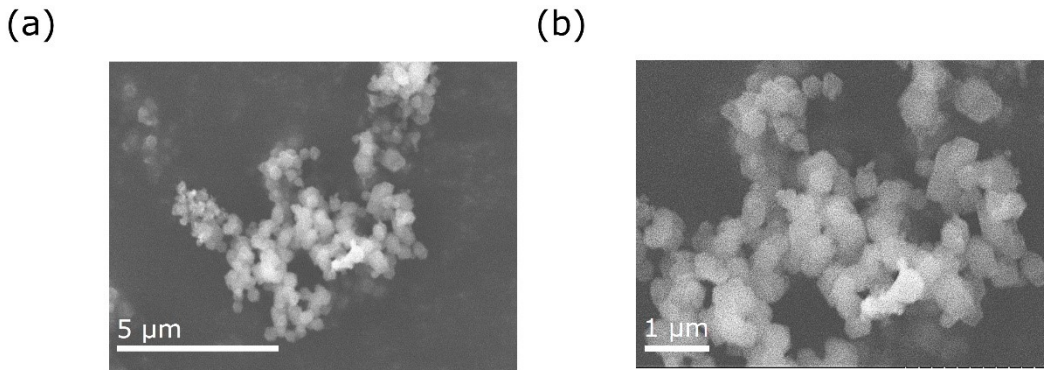

Fig. S2. SEM images of the ZIF-67.

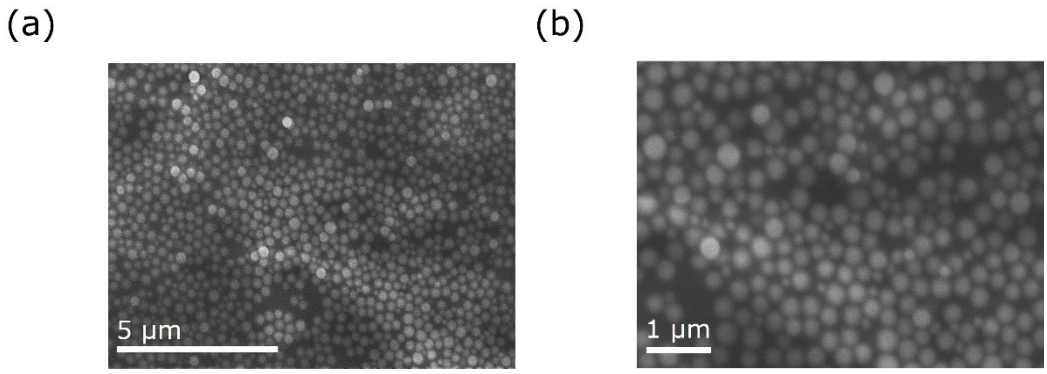

Fig. S3. SEM images of the SiO_2.

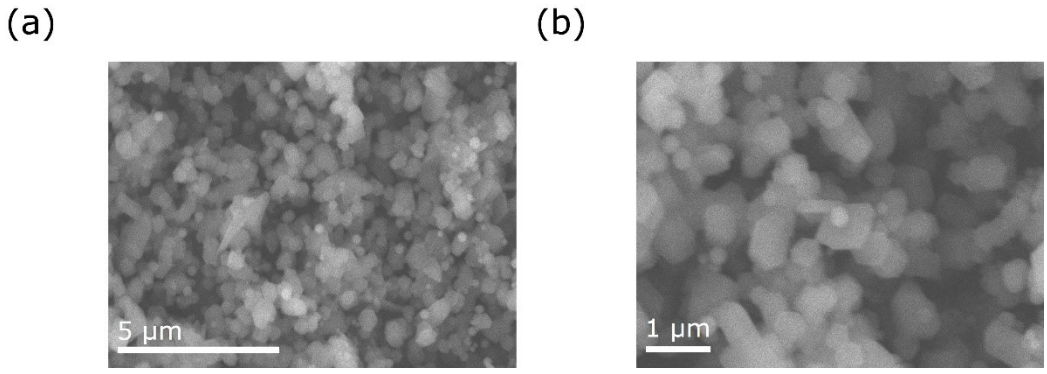

Fig. S4. SEM images of the ZIF-67@SiO_2.

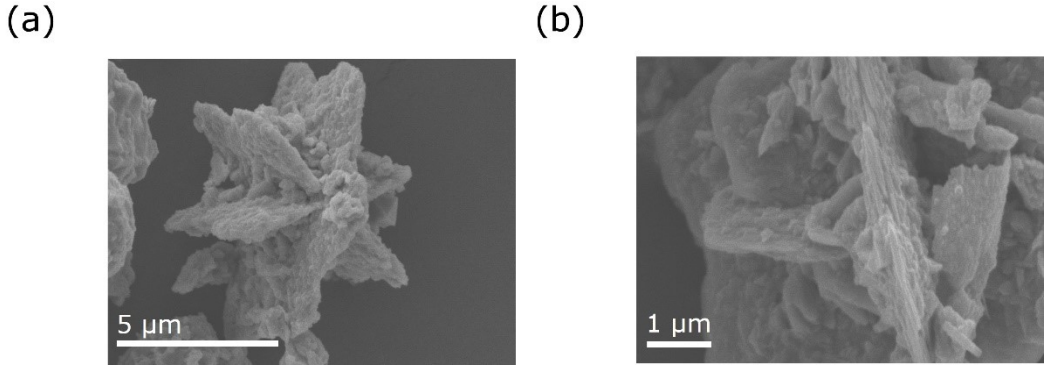

Fig. S5. SEM images of the Co_1/Ni_1-S.

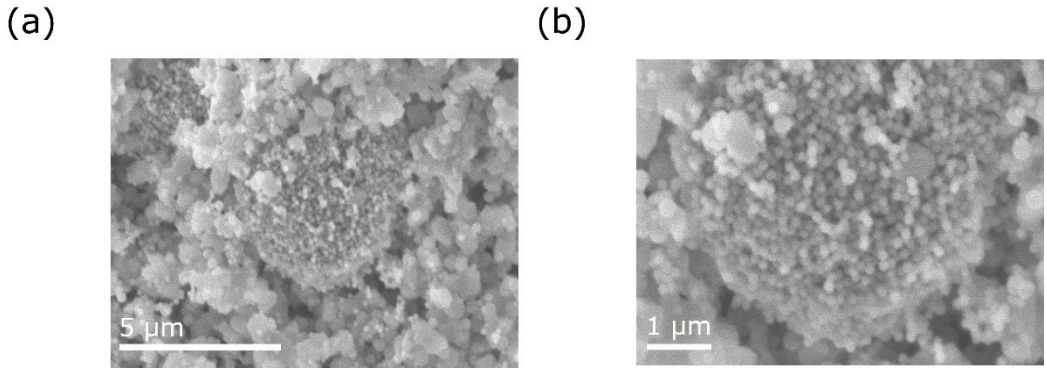

Fig. S6. SEM images of the ZIF-67@SiO_2@Co_1/Ni_1-S.

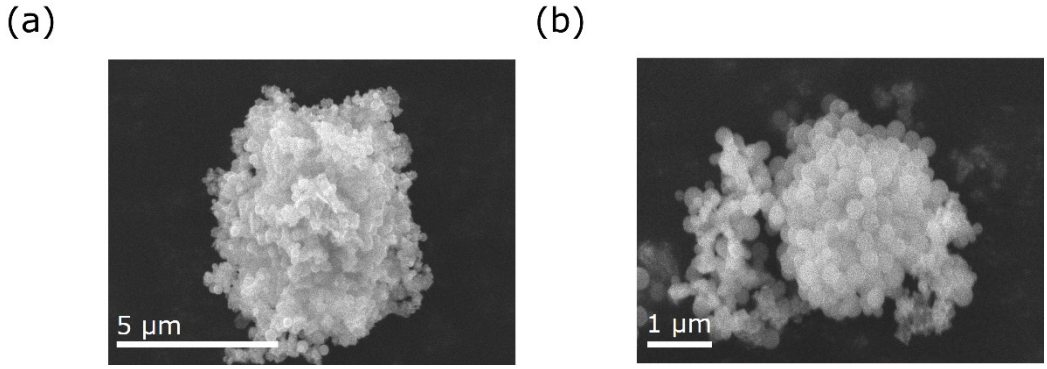

Fig. S7. SEM images of the $Ni_3S_2/Co_9S_8/SiO_2$@Co-NC.

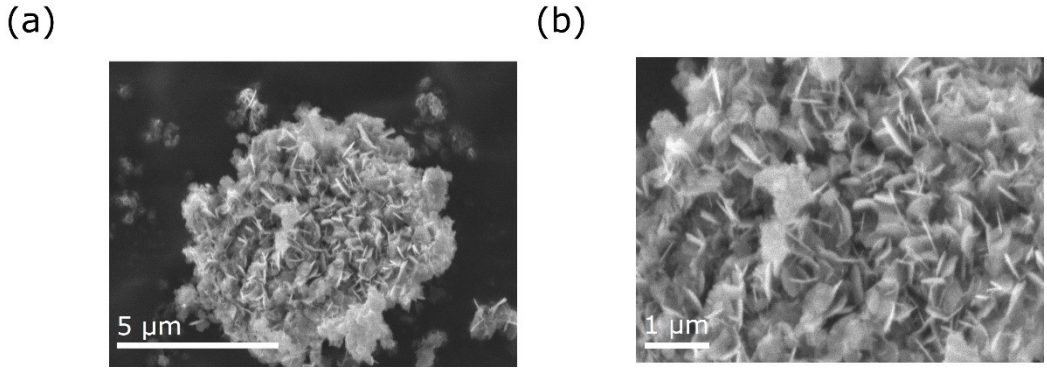

Fig. S8. SEM images of the Ni_3S_2/Co_9S_8@Co-NC.

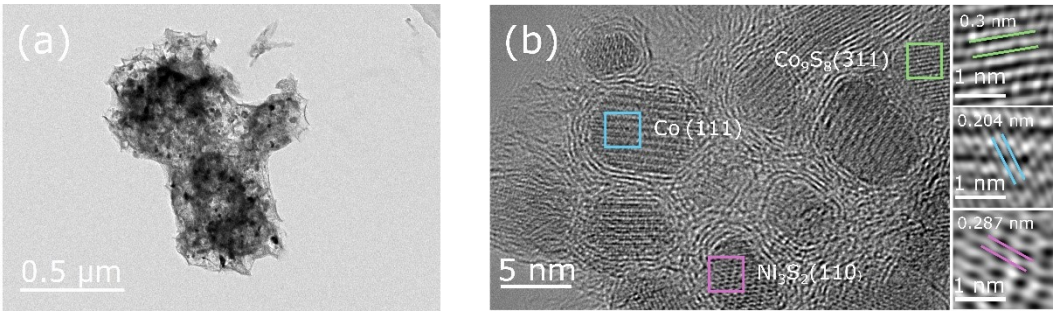

Fig. S9. TEM image of Ni_3S_2/Co_9S_8@Co-NC.

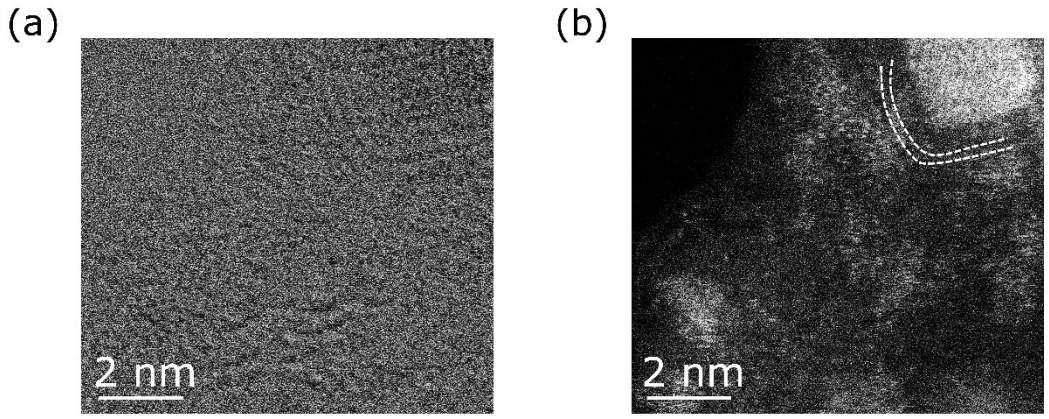

Fig. S10. Bright field (a) and dark field (b) aberration-corrected HAADF-STEM images for Ni_3S_2/Co_9S_8@Co-NC.

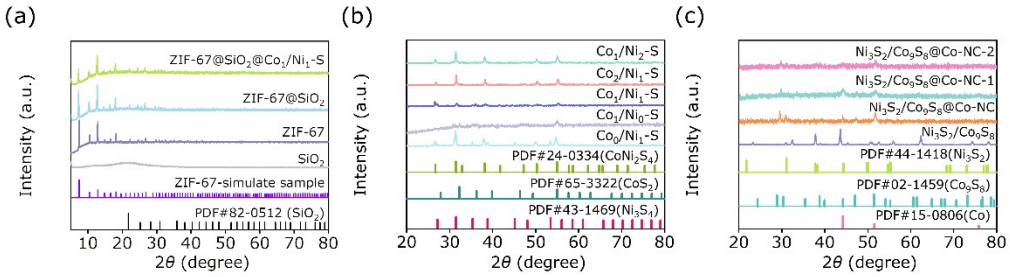

Fig. S11. Powder XRD patterns of as-prepared precursor **(a)**, **(b)**, Ni_3S_2/Co_9S_8, Ni_3S_2/Co_9S_8@Co-NC and Ni_3S_2/Co_9S_8@Co-NC-x (x=1, 2) **(c)**.

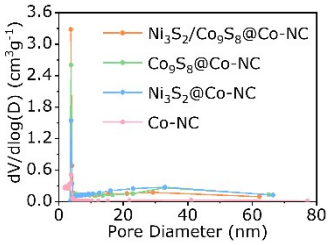

Fig. S12. The pore size distribution curves of different samples.

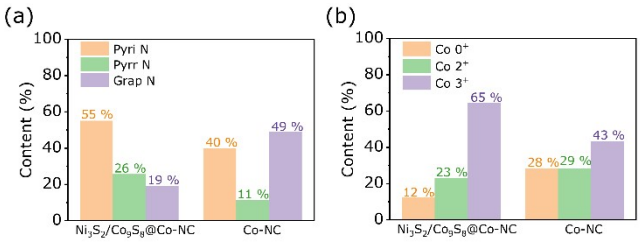

Fig. S13. (a) N 1s and **(b)** Co 2p corresponding high-resolution XPS spectra of fitting peak area data.

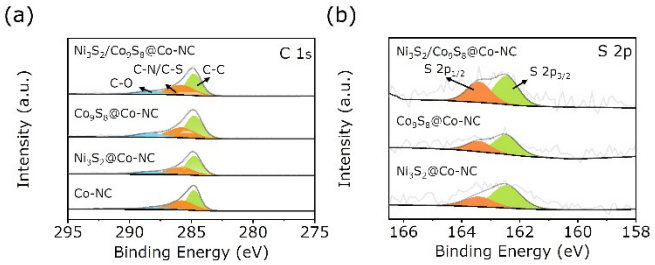

Fig. S14. (a) C 1s and **(b)** S 2p high-resolution XPS spectra of different samples along with the corresponding fitting curves.

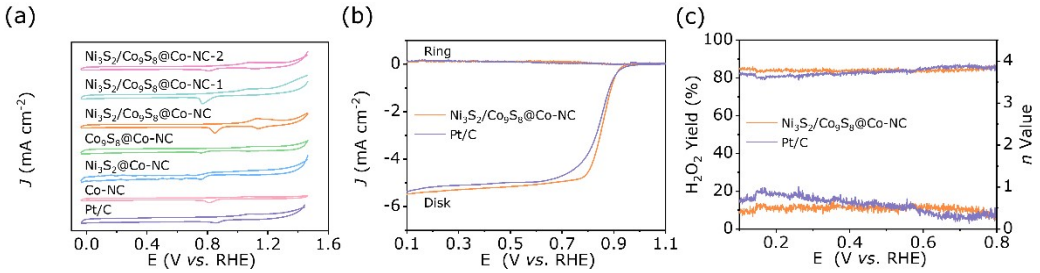

Fig. S15. (a) CV curves of Ni_3S_2/Co_9S_8@Co-NC, Ni_3S_2/Co_9S_8@Co-NC-x (x=1, 2), Co_9S_8@Co-NC, Ni_3S_2@Co-NC, Co-NC and Pt/C in an O_2-saturated at 10 mV s^{-1}; **(b)** RRDE voltammograms of Ni_3S_2/Co_9S_8@Co-NC and Pt/C in O_2-saturated; **(c)** H_2O_2 yields and the corresponding electron transfer number (n) of Ni_3S_2/Co_9S_8@Co-NC and Pt/C.

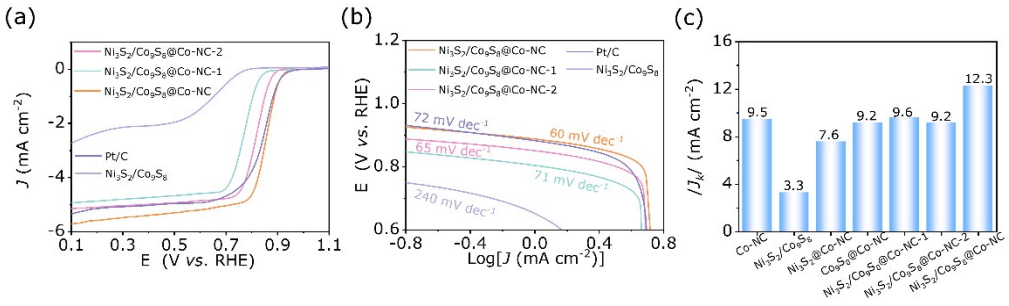

Fig. S16. (a) LSV curves of Ni_3S_2/Co_9S_8, Ni_3S_2/Co_9S_8@Co-NC, Ni_3S_2/Co_9S_8@Co-NC-x (x=1, 2) and Pt/C in an O_2-saturated 0.1 M KOH solution at 2 mV s^{-1} and corresponding tafel plots **(b)**; **(c)** Kinetic current density (J_K) of different samples.

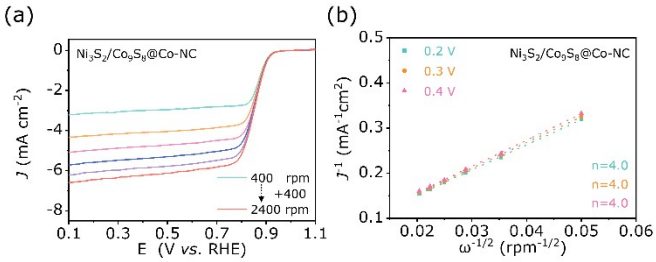

Fig. S17. LSV curves at different rotation rates (400-2400 rpm) of **(a)** Ni_3S_2/Co_9S_8@Co-NC and corresponding K-L plots **(b)**.

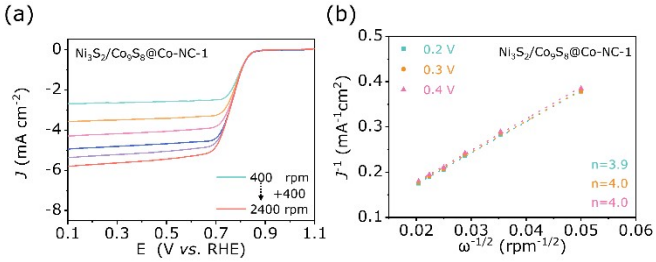

Fig. S18. LSV curves at different rotation rates (400-2400 rpm) of **(a)** Ni_3S_2/Co_9S_8@Co-NC-1 and corresponding K-L plots **(b)**.

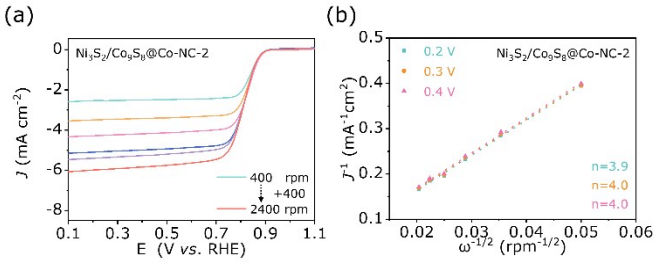

Fig. S19. LSV curves at different rotation rates (400-2400 rpm) of **(a)** Ni_3S_2/Co_9S_8@Co-NC-2 and corresponding K-L plots **(b)**.

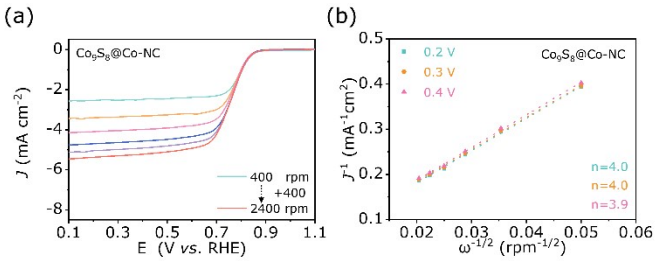

Fig. S20. LSV curves at different rotation rates (400-2400 rpm) of **(a)** Co_9S_8@Co-NC and corresponding K-L plots **(b)**.

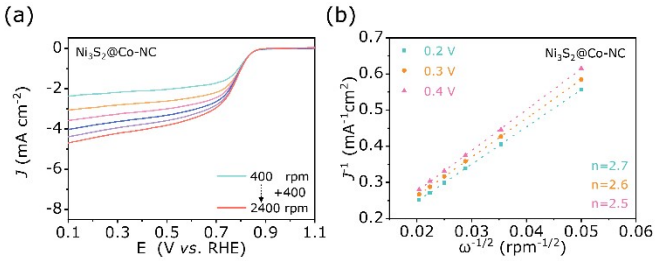

Fig. S21. LSV curves at different rotation rates (400-2400 rpm) of **(a)** Ni_3S_2@Co-NC and corresponding K-L plots **(b)**.

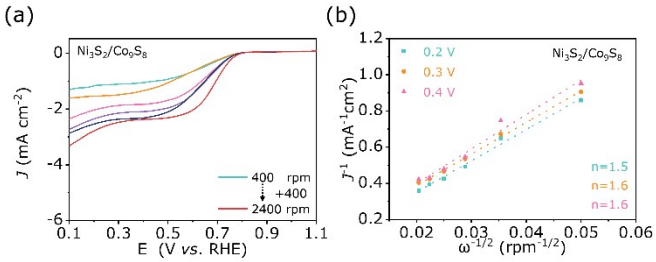

Fig. S22. LSV curves at different rotation rates (400-2400 rpm) of **(a)** Ni_3S_2/Co_9S_8 and corresponding K-L plots **(b)**.

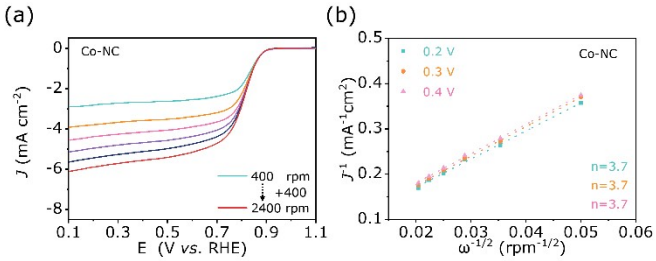

Fig. S23. LSV curves at different rotation rates (400-2400 rpm) of **(a)** Co-NC and corresponding K-L plots **(b)**.

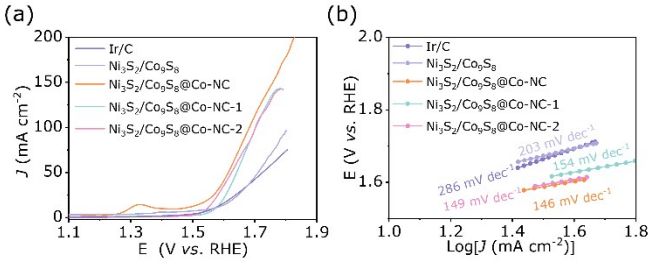

Fig. S24. (a) LSV curves of Ni_3S_2/Co_9S_8, Ni_3S_2/Co_9S_8@Co-NC, Ni_3S_2/Co_9S_8@Co-NC-x (x=1, 2) and Ir/C in 1 M KOH solution at 20 mV s^{-1} and corresponding tafel plots **(b)** for OER.

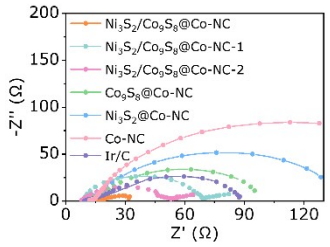

Fig. S25. Nyquist curves of Ni_3S_2/Co_9S_8@Co-NC, Ni_3S_2/Co_9S_8@Co-NC-x (x=1, 2), Co_9S_8@Co-NC, Ni_3S_2@Co-NC, Co-NC and Ir/C.

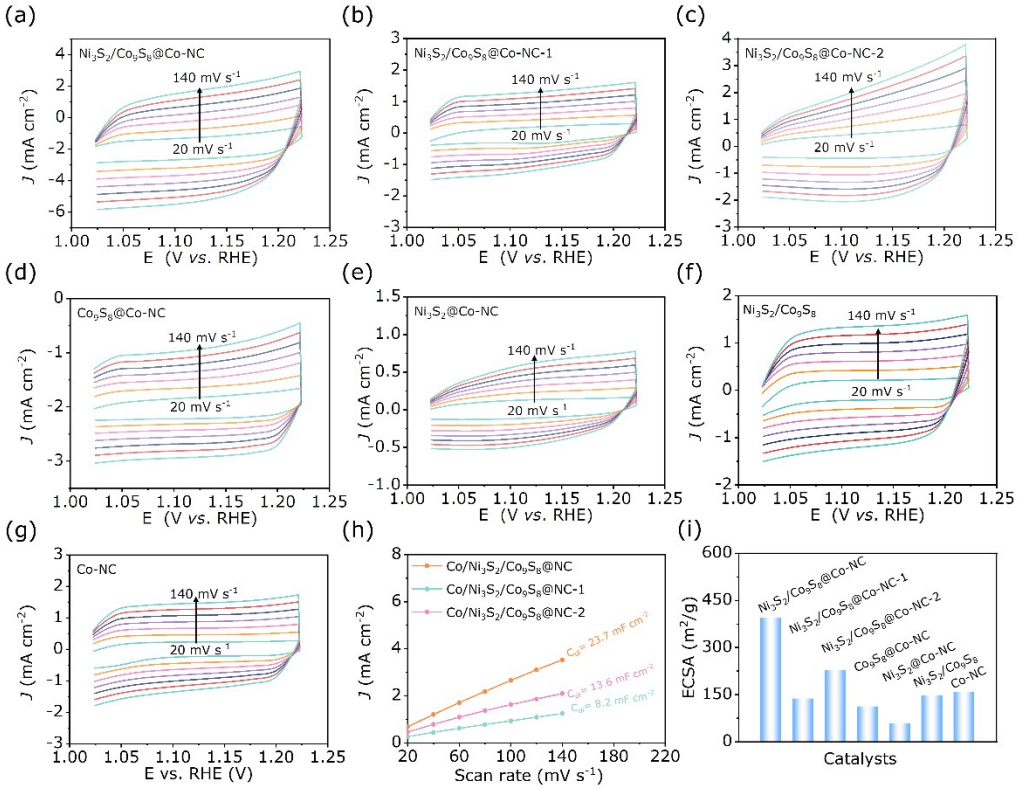

Fig. S26. Cyclic voltammetry (CV) curves of **(a)** Ni_3S_2/Co_9S_8@Co-NC, **(b)** Ni_3S_2/Co_9S_8@Co-NC-1, **(c)** Ni_3S_2/Co_9S_8@Co-NC-2, **(d)** Co_9S_8@Co-NC, **(e)** Ni_3S_2@Co-NC, **(f)** Ni_3S_2/Co_9S_8, **(g)** Co-NC at varied with different scan rates from 20 to 140 $mV \cdot s^{-1}$ in a non-faradic potential range of 1.02~1.22 V vs. RHE; **(h)** Double-layer capacitance (C_{dl}) and **(i)** electrochemical active surface area (ECSA) of different samples.

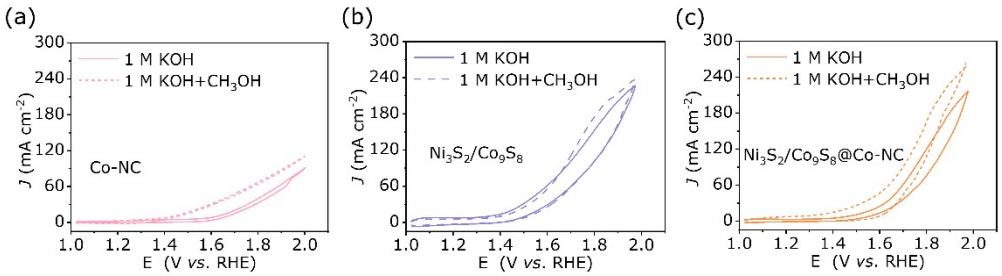

Fig. S27. CV curves for **(a)** Co-NC, **(b)** Ni_3S_2/Co_9S_8 and **(c)** Ni_3S_2/Co_9S_8@Co-NC in 1 M KOH with and without methanol (1 M).

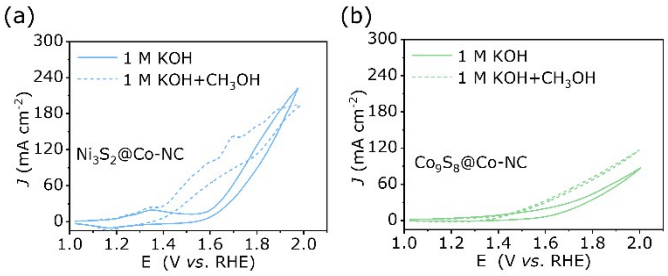

Fig. S28. CV curves for **(a)** Ni_3S_2@Co-NC and **(b)** Co_9S_8@Co-NC in 1 M KOH with and without methanol (1 M).

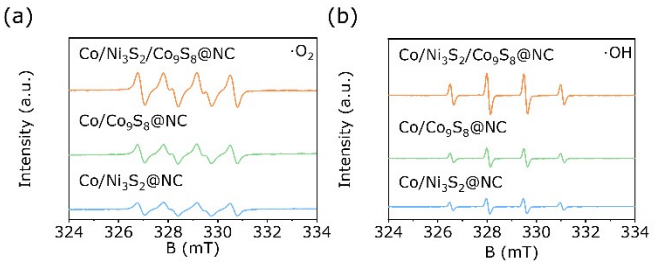

Fig. S29. (a) ESR spectra of the Ni_3S_2/Co_9S_8@Co-NC•O; **(b)** ESR spectra of the Ni_3S_2/Co_9S_8@Co-NC-•OH.

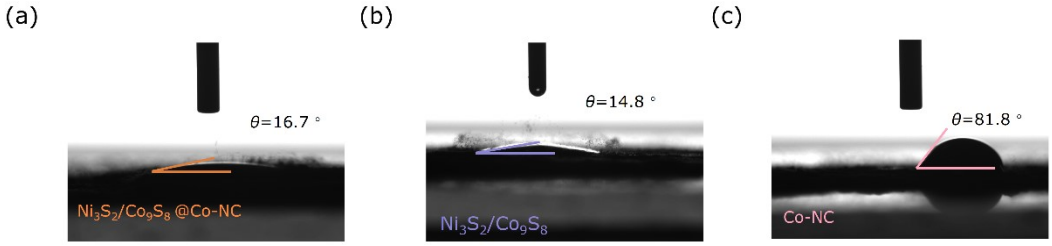

Fig. S30. Contact angles of **(a)** Ni_3S_2/Co_9S_8@Co-NC, **(b)** Ni_3S_2/Co_9S_8 and **(c)** Co-NC.

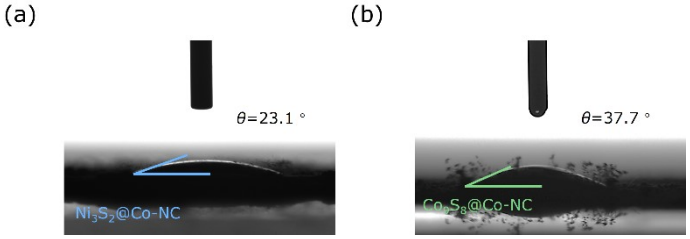

Fig. S31. Contact angles of **(a)** Ni_3S_2@Co-NC and **(b)** Co_9S_8@Co-NC.

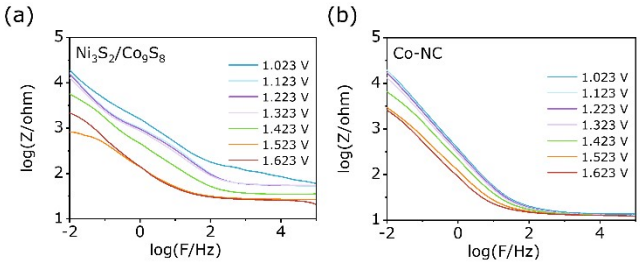

Fig. S32. The Bode frequency plots of the in-situ electrochemical impedance spectroscopy on **(a)** Ni_3S_2/Co_9S_8 and **(b)** Co-NC.

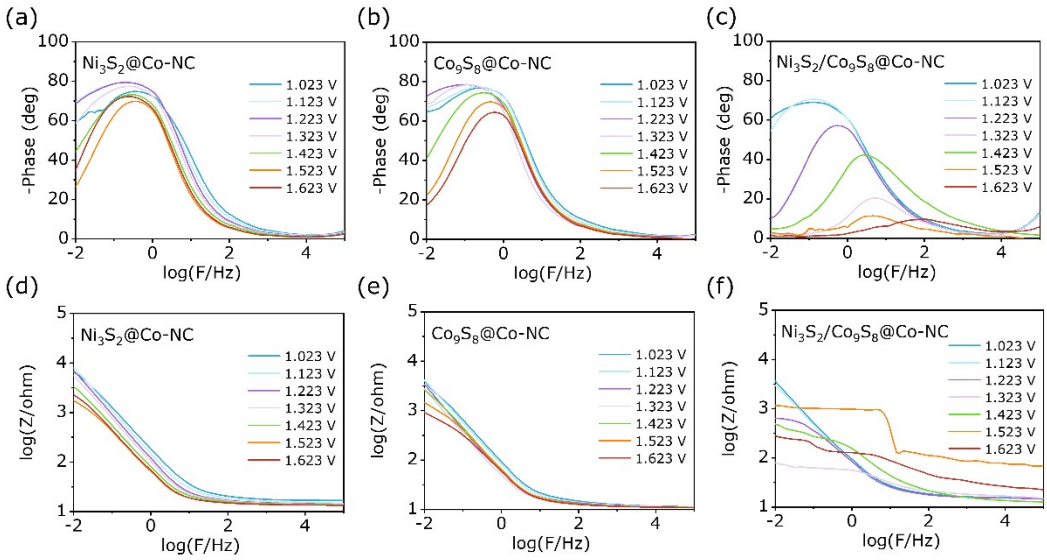

Fig. S33. The Bode phase plots of the in-situ electrochemical impedance spectroscopy on **(a)** Ni_3S_2@Co-NC, **(b)** Co_9S_8@Co-NC, **(c)** Ni_3S_2/Co_9S_8@Co-NC and corresponding the Bode frequency plots **(d)**, **(e)**, **(f)**.

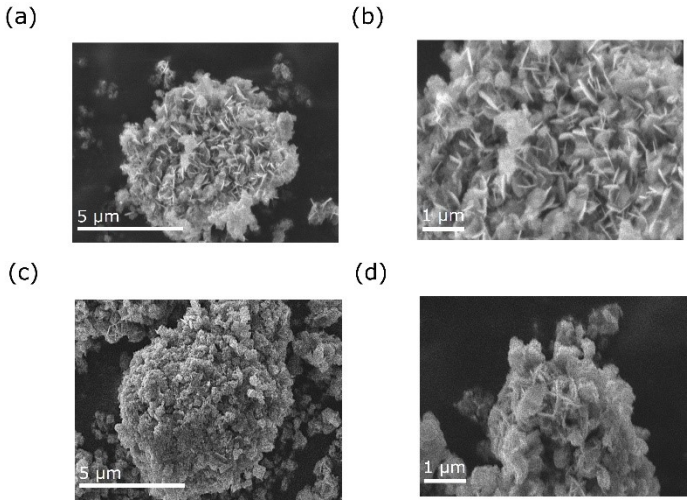

Fig. S34. SEM for initial Ni_3S_2/Co_9S_8@Co-NC **(a)**, **(b)** and after 20 h charging/discharging cycling stability test at 30 mA cm^{-2} **(c)**, **(d)**.

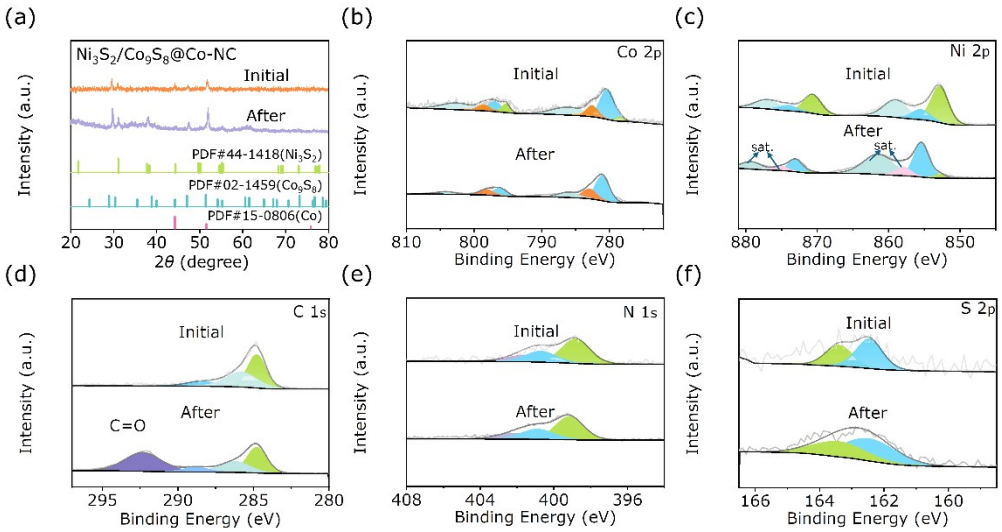

Fig. S35. XRD **(a)** patterns and XPS patterns **(b)** Co 2p, **(c)** Ni 2p, **(d)**N 1s, **(e)** C 1s, **(f)** S 2p for Ni_3S_2/Co_9S_8@Co-NC catalysts after 20 h charging/discharging cycling stability test at 30 mA cm^{-2}.

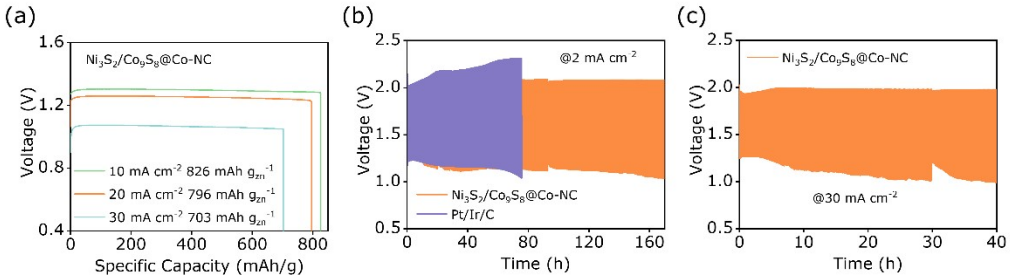

Fig. S36. (a) Specific capacities curves for Ni_3S_2/Co_9S_8@Co-NC-based ZAB at different current densities. **(b)** The charging/discharging cycling curves for Ni_3S_2/Co_9S_8@Co-NC-based ZAB and Pt/Ir/C-based ZAB at 2 mA cm^{-2}. **(c)** The charging/discharging cycling curves for Ni_3S_2/Co_9S_8@Co-NC-based ZAB at 30 mA cm^{-2}.

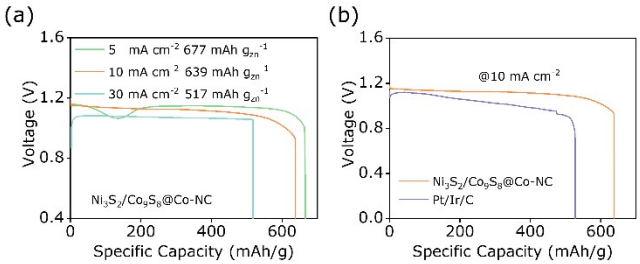

Fig. S37. Specific capacities curves for Ni_3S_2/Co_9S_8@Co-NC-based FZAB at different current densities **(a)** and comparison with Pt/Ir/C at 10 mA cm^{-2} **(b)**.

Section 3. Supporting tables.

Table S1. The electrocatalytic activities of recently reported bifunctional electrocatalysts for OER and ORR.

Catalysts	Half-wave potential ($E_{1/2}$, mV)	Potential at 10 mA cm^{-2} ($E_{j=10}$, mV)	Potential difference between $E_{1/2}$ and $E_{j=10}$ (ΔE, mV)	Ref
Ni_3S_2/Co_9S_8@Co-NC	854	1486	632	This work
NiFeVS	789	1594	805	[1]
CoNP@FeNC-0.05	850	1630	780	[2]
$Fe_8Co_{0.2}$-NC-800	820	1632	812	[3]
NCMS/NrGO	830	1590	760	[4]
FeNiCo|$MnGaO_x$	824	1485	661	[5]
SPAN-FCNM	710	1440	730	[6]
$Fe_{1.2}(CoNi)_{1.8}S_6$	810	1476	666	[7]
Co_3S_4/FeS@CoFe/NC	872	1490	618	[8]
Co-Ni-S@NSPC	820	1700	880	[9]
$Fe_{0.20}Co_{0.80}P$/PNC	828	1545	717	[10]
Mo-Co/N-C	869	1579	710	[11]
$NiCo_2S_4$/HCS	890	1540	650	[12]

Reference

1. F. N. I. Sari, Y. C. Lai, Y. J. Huang, X. Y. Wei, H. Pourzolfaghar, Y. H. Chang, M. Ghufron, Y. Y. Li, Y. H. Su and O. Clemens, *Adv. Funct. Mater.*, 2024, **34**, 2310181.
2. Y. Xue, Y. Guo, Q. Zhang, Z. Xie, J. Wei and Z. Zhou, *Nano Micro Lett.*, 2022, **14**, 162.
3. T. Jin, J. Nie, M. Dong, B. Chen, J. Nie and G. Ma, *Nano Micro Lett.*, 2023, **15**, 26.
4. J. S. Sanchez, Z. Xia, K. Mirehbar, S. Sasidharan, S. A. Aravindh, A. Liscio, J. Sun, M. Christian, J. Palma and V. Palermo, *J. Mater. Chem. A*, 2024, **12**, 11945-11959.
5. L. Luo, Y. Liu, S. Chen, Q. Zhu, D. Zhang, Y. Fu, J. Li, J. Han and S. Gong, *Small*, 2024, **20**, 2308756.
6. C.-L. Huang, Z.-F. He, J.-Y. Pai, Y.-H. Yang, W.-Y. Jao, C.-Y. Lai, Y.-T. Lu, H.-Y. Ku and C.-C. Hu, *Chem. Eng. J.*, 2023, **469**, 143855.
7. H. Wu, Z. Li, Z. Wang, Y. Ma, S. Huang, F. Ding, F. Li, Q. Zhai, Y. Ren and X. Zheng, *Appl. Catal. B Environ.*, 2023, **325**, 122356.
8. Y. Tan, Y. Wang, A. Li, X. Jiang, Y. Zhang and C. Cheng, *J. Energy Chem.*, 2024, **96**, 568-577.
9. W. Fang, H. Hu, T. Jiang, G. Li and M. Wu, *Carbon*, 2019, **146**, 476-485.
10. X. W. Gao, J. J. Mu, R. Wei, X. Wang, Q. Gu, L. K. Zhao and W. B. Luo, *Small Methods*, 2024, **8**, 2301645.
11. Y. Zhang, X. Ma, Z. Cheng, J. Wang, G. Wen, L. Yang and Z. Bai, *Adv. Funct. Mater.*, 2024, **34**, 2314622.
12. J. Liu, X. Meng, J. Xie, B. Liu, B. Tang, R. Wang, C. Wang, P. Gu, Y. Song and S. Huo, *Adv. Funct. Mater.*, 2023, **33**, 2300579.